Electrochemistry

DOI: 10.1002/anie.201206789

Electrodeposition of Crystalline and Photoactive Silicon Directly from Silicon Dioxide Nanoparticles in Molten $CaCl_2$**

*Sung Ki Cho, Fu-Ren F. Fan, and Allen J. Bard**

Silicon is a widely used semiconductor for electronic and photovoltaic devices because of its earth-abundance, chemical stability, and the tunable electrical properties by doping. Therefore, the production of pure silicon films by simple and inexpensive methods has been the subject of many investigations. The desire for lower-cost silicon-based solar photovoltaic devices has encouraged the quest for solar-grade silicon production through processes alternative to the currently used Czochralski process or other processes.

Electrodeposition is one of the least expensive methods for fabricating films of metals and semiconductors. Electrodeposition of silicon has been studied for over 30 years, in various solution media such as molten salts (LiF-KF-K_2SiF_6 at 745 °C[1,2] and BaO-SiO_2-BaF_2 at 1465 °C[3,4]), organic solvents (acetonitrile, tetrahydrofuran),[5] and room-temperature ionic liquids.[6] Recently, the direct electrochemical reduction of bulk solid silicon dioxide in a $CaCl_2$ melt was reported.[7] A key factor for silicon electrodeposition is the purity of silicon deposit because Si for the use in photovoltaic devices is solar-grade silicon (> 99.9999 % or 6N) and its grade is even higher in electronic devices (electronic-grade silicon or 11N). In most cases, the electrodeposited silicon does not meet these requirements without further purification and, to our knowledge, none have been shown to exhibit a photoresponse.

In fact, silicon electrodeposition is not as straightforward as metal deposition, since the deposited semiconductor layer is resistive at room temperature, which complicates electron transfer through the deposit. In many cases, for example in room-temperature aprotic solvents, the deposited silicon acts as an insulating layer and prevents a continuous deposition reaction.[5] In some cases, the silicon deposit contains a high level of impurities (> 2 %). Moreover, the nucleation and growth of silicon requires a large amount of energy. The deposition is made even more challenging if the Si precursor is SiO_2, which is a very resistive material.

We reported previously[8] the electrochemical formation of silicon on molybdenum from a $CaCl_2$ molten salt (850 °C) containing a SiO_2 nanoparticle (NP with a diameter of 5–15 nm) suspension by applying a constant reduction current. However this Si film did not show photoactivity. Here we show the electrodeposition of photoactive crystalline silicon directly from SiO_2 NPs from $CaCl_2$ molten salt on a silver electrode that shows a clear photoresponse. To the best of our knowledge, this is a first report of the direct electrodeposition of photoactive silicon.

The electrochemical reduction and the cyclic voltammetry (CV) of SiO_2 were investigated as described previously.[8] In this study, we found that the replacement of the Mo substrate by silver leads to a dramatic change in the properties of the silicon deposit. The silver substrate exhibited essentially the same electrochemical and CV behavior as other metal substrates, that is, a high reduction current for SiO_2 at negative potentials of −1.0 V with the development of a new redox couple near −0.65 V vs. a graphite quasireference electrode (QRE) (Figure 1 a). Figure 1 b shows a change in the reduction current as a function of the reduction potential, and the optical images of silver electrodes before and after the electrolysis, which displays a dark gray-colored deposit after the reduction. Figure 2 shows SEM images of silicon deposits grown potentiostatically (−1.25 V vs. graphite QRE) on silver. The amount of silicon deposit increased with the deposition time, and the deposit finally covered the whole silver surface (Figure 2). High-magnification images show that the silicon deposit is not a film but rather platelets or clusters of silicon crystals of domain sizes in the range of tens of micrometers. The average height of the platelets was around 25 μm after a 10000 s deposition (Figure 2 b), and 45 μm after a 20000 s deposition (Figure 2 c), respectively. The edges of the silicon crystals were clearly observed. Contrary to other substrates,[8] silver enhanced the crystallization of silicon produced from silicon dioxide reduction and it is known that silver induces the crystallization of amorphous silicon.[9]

Energy-dispersive spectrometry (EDS) elemental mapping (images shown in the bottom row of Figure 2) revealed that small silver islands exist on the top of the silicon deposits, which we think is closely related to the growth mechanism of silicon on silver. The EDS spectrum of the silicon deposit (Figure 3 a) suggested that the deposited silicon was quite pure and the amounts of other elements such as C, Ca, and Cl were below the detection limit (about 0.1 atom %). Since the oxygen signal was probably from the native oxide formed on exposure of the deposit to air and silicon does not form an alloy with silver, the purity of silicon was estimated to be at least 99.9 atom %. The successful reduction of Si(4+) in silicon dioxide to elemental silicon (Si^0) was confirmed by X-ray photoelectron spectroscopy (XPS) of the silicon deposit

[*] Dr. S. K. Cho, Dr. F.-R. F. Fan, Prof. A. J. Bard
Center for Electrochemistry, Department of Chemistry and Biochemistry, The University of Texas at Austin
Austin, TX 78712 (USA)
E-mail: ajbard@mail.utexas.edu

[**] We appreciate financial support of this project from the Dow Corning Corporation, the Robert A. Welch Foundation (grant numbers F-0032 and H-F-0037) and the Center for Electrochemistry. We are grateful for the assistance of Dr. Rob Morgan and Dr. Dimi Katsoulis at Dow Corning in the ICP-MS analysis.

Supporting information for this article is available on the WWW under http://dx.doi.org/10.1002/anie.201206789.

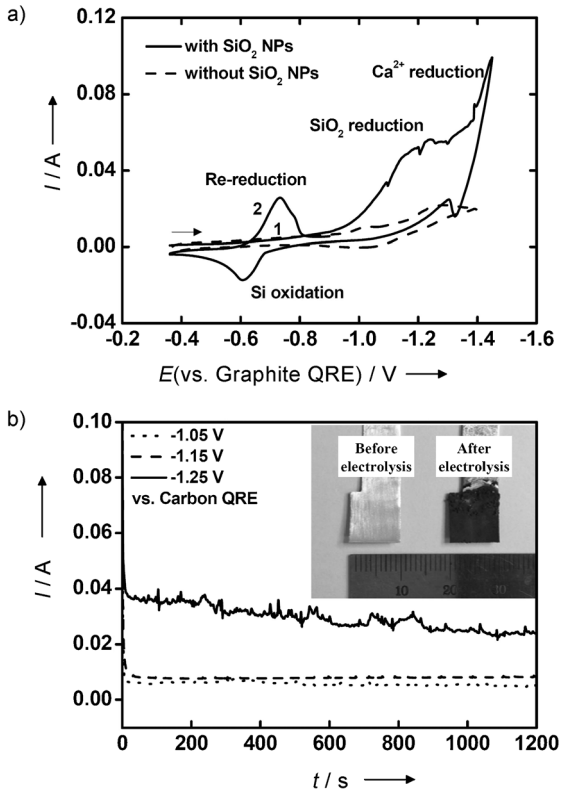

Figure 1. a) Cyclic voltammograms on the silver electrode (about 2 cm^2) at a scan rate of 20 $mV s^{-1}$ and b) chronoamperograms at a silver electrode with various applied potentials (vs. a quasireference electrode) in a 850 °C $CaCl_2$ melt containing a suspension of 0.2 M SiO_2 NPs and the optical images of silver electrodes before and after electrodeposition (−1.25 V vs. graphite quasireference electrode, 10000 s).

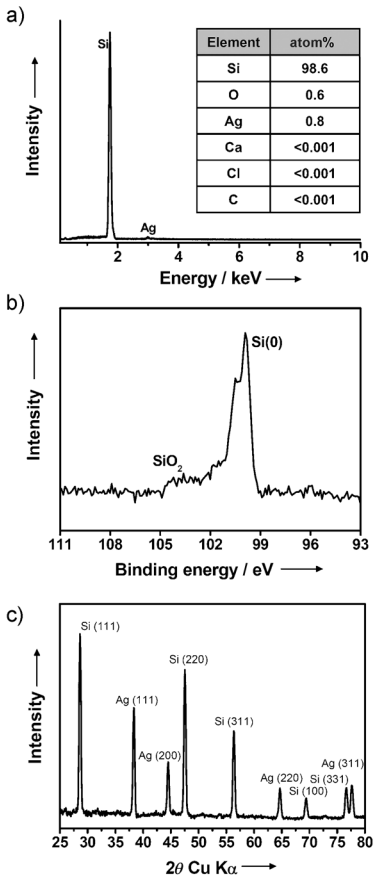

Figure 3. a) EDS spectrum, b) X-ray photoelectron spectrum, and c) θ-2θ X-ray diffraction spectrum of a silicon deposit grown at −1.25 V vs. a graphite quasireference electrode on a silver substrate in a 850 °C $CaCl_2$ melt containing 0.2 M SiO_2 nanoparticles.

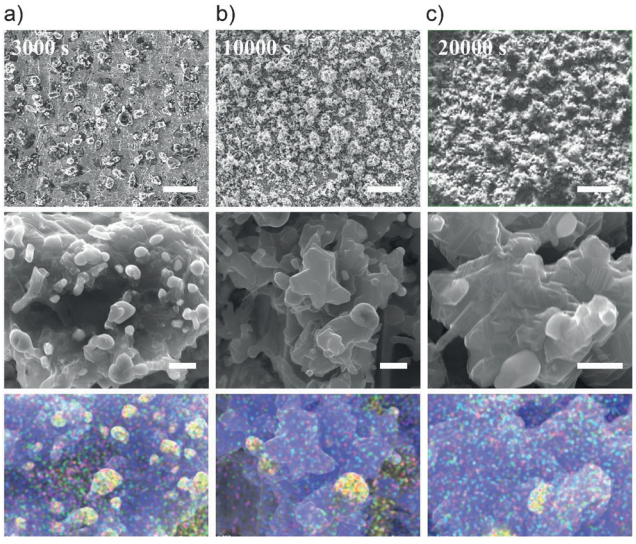

Figure 2. SEM images of Si deposited at −1.25 V vs. a graphite quasireference electrode on a silver substrate for a) 3000, b) 10000, and c) 20000 s in a 850 °C $CaCl_2$ melt containing 0.2 M SiO_2 nanoparticles. The scales of the white bars are 50 μm (top row) and 2 μm (middle row), respectively. The bottom row shows EDS element mapping images of the middle row, in which the blue area corresponds to silicon and the yellow area corresponds to silver.

(Figure 3b), and X-ray diffraction (XRD) analysis indicates that the silicon deposit is polycrystalline (Figure 3c).

Photoactivity is the key characteristic of silicon for use as a solar material and its presence demonstrates sufficient purity for solar photovoltaic applications. While studies of solid-state emission of Si usually involves fabricating a p–n junction and a cell, we have previously shown in studies of $CuInSe_2$ and $CuIn_{1-x}Ga_xSe_2$ thin films that PEC measurements of the semiconductor material with a liquid junction correlates well with the observed behavior in solid-state photovoltaic cells.[10] Thus, we determined the photoresponse of the silicon deposit in an aprotic solvent, acetonitrile (to prevent any reaction with water) in an electrolyte solution containing 50 mM ethyl viologen (EV^{2+}), the reduction potential of which is within the band gap of silicon. Immersion of silicon deposit in the electrolyte formed a semiconductor-liquid junction, where changes in the redox reaction current of the photoelectrode with potential under irradiation with UV/Vis light can be detected. Figure 4 shows the change in the open circuit potential and the linear sweep voltammetry of the silicon deposit on silver under xenon lamp (100 $mW cm^{-2}$) radiation. In Figure 4a, the open circuit potential of the silicon deposit in EV^{2+} solution shifted in the positive direction under irradiation, indicating this silicon

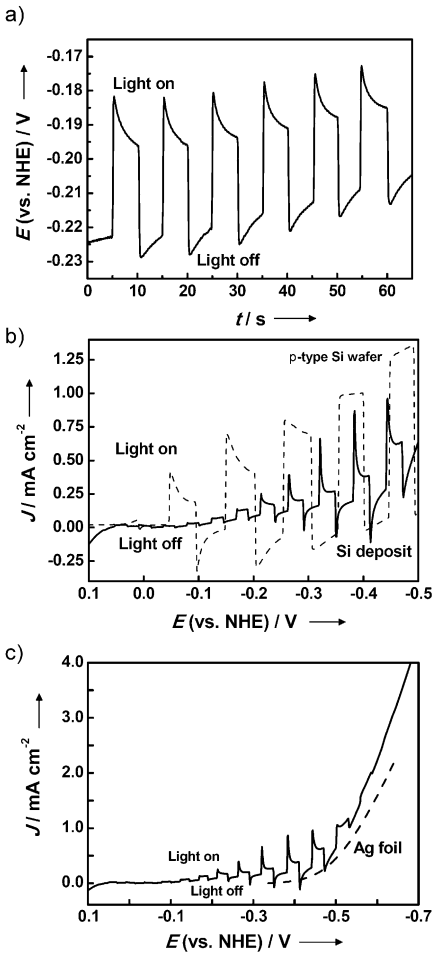

Figure 4. The photoresponse of a silicon deposit measured in a PEC cell. a) The open circuit potential of the silicon deposit with light on or off. b) A recording of the photocurrent of the silicon deposit as a function of the applied potential with and without light irradiation. c) Same as (b) but scanning the potential to a more negative value; the dashed curve is the voltammetric curve on a bare silver electrode. The electrolyte was an acetonitrile solution containing 0.1 M tetrabutylammonium hexafluorophosphate and 0.05 M ethyl viologen diperchlorate. A xenon lamp with 100 mW cm^{-2} light intensity was used as the light source. The electrical contact was made on the silver substrate. The dotted line in (b) represents the current–potential behavior of a silicon wafer [0.27 cm^2 exposed active area, 3 Ω cm resistivity, p-type, (100)] measured in the same PEC cell with and without light illumination. The electric contact was made on the backside of the silicon wafer with silver paste, which gives a contact configuration the same as the silicon deposit on silver.

deposit is a p-type semiconductor. A recording of the photocurrent for the photoreduction of EV^{2+} as a function of applied potential is shown in Figure 4b. An increase in the reduction current with the light illumination was observed, also indicating p-type behavior of the silicon deposit. A commercial p-type single-crystal silicon wafer under identical measurement conditions showed a potential shift in the same direction and a reduction current with illumination (Figure 4b and Figure S2 in Supporting Information). The onset potential for the photocurrent (near the flat-band potential) of the silicon deposit was around 0.05 V (vs. the normal hydrogen electrode, NHE) which is almost the same as that observed for the silicon wafer. The sharp decrease in the photocurrent after the instantaneous increase under irradiation was perhaps due to the silver islands, which could enhance the recombination of photogenerated electrons and holes. At −0.4 V (vs. NHE), the peak photocurrent was about 0.75 mA cm^{-2} and was saturated to 0.35 mA cm^{-2} whereas the silicon wafer exhibited about 1.0 mA cm^{-2}. The evolution of the oxidation current after cutoff of illumination might be from the re-oxidation of EV^+ on exposed silver islands and the substrate electrode. As the potential became more negative, the dark current increased, which also indicates the reduction of EV^{2+} on silver, as the same current was observed on a bare silver surface (Figure 4c).

The minimum purity of deposited silicon was 99.9 atom % according to the EDS analysis. However the clear photoresponse of the silicon deposit, at roughly half the maximum photocurrent as a pure Si wafer, is also indicative of its high purity. The trace amounts of impurities and probable dopant for the p-type behavior were examined by time-of-flight secondary-ion mass spectrometry (TOF-SIMS). Figure 5 exhibits the depth profiles and the surface mappings of elements detected on the silicon deposit in the positive and negative ion modes of SIMS. Although almost all elements from $CaCl_2$, Ag, SiO_2, and their impurities were detected, most of them have a count number of less than one at each sputtering cycle (about 1.6 s) during depth profiling. After running through the whole spectrum, elements, which showed noticeable counts were selected and are shown (Figure S4 in the Supporting Information). Perceptible counts from Ag, Ca, C, and Cl were detected and their counts decreased gradually with Cs^+ sputtering, while the silicon counts remained constant, indicating that these largely contaminated the silicon surface (Figure 5). Similarly, the counts of trace impurities, such as Mg, Fe, and Mn also decreased with the sputtering and almost disappeared in 200 s which corresponds to removal of 20 nm of silicon (Figure S4 in the Supporting Information), indicating that those elements are also on or near surface. Elemental mapping was carried on after Cs^+ sputtering for 1500 s (about 150 nm) to remove the surface impurities. In elemental mappings, the shape of the silicon region (reddish brown area) was similar to the morphology in SEM images, and each element had a unique and distinct distribution. The distribution pattern of silver did not follow that of silicon and it was highly localized as shown as silver islands in SEM images (Figure 2). Ca and Cl existed separately from silicon and silver, whereas their distribution were very similar to each other, indicating that they are from small amounts of $CaCl_2$ left on the surface after cleaning the electrode after removal. Carbon, a possible contaminant from the graphite counter electrode, also had a different distribution from silicon. We conclude that Ag, Ca, Cl, and C exist predominantly on the surface and were not detrimental impurities in our silicon crystal after surface etching.

The contaminated surface caused difficulty in a quantitative determination of purity of the bulk silicon deposit by inductively coupled plasma mass spectroscopy (ICP-MS), as the deposited silicon platelet has a large surface area and mainly surface impurities relative to a silicon wafer. Herein,

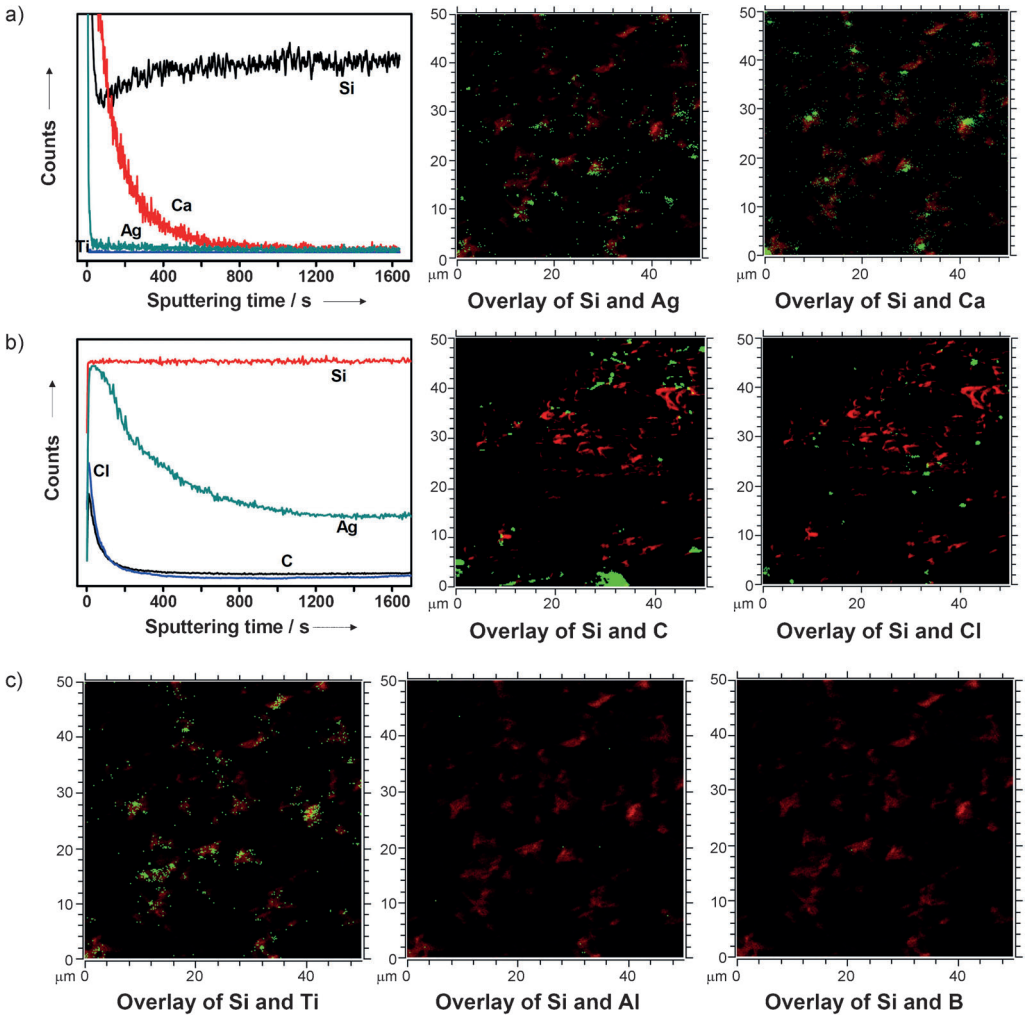

Figure 5. Secondary ion mass spectroscopic depth profiles and elemental mappings of silicon deposit in a) positive ion and b) negative ion mode. Si, Ag, and Ca have a positive ion polarity whereas C and Cl have a negative ion polarity. Elemental mappings were performed after Cs^+ sputtering for 1500 s. In mapping images, reddish brown area indicates Si regions, and bright green spots indicate Ag, Ca, C, and Cl regions, which are overlaid on Si. c) Elemental mappings of silicon deposit with Ti, Al, and B.

ICP-MS on the silicon deposit showed 1600 ppm of total impurity, which corresponds to 99.8 wt. % silicon purity (see Table S1 in the Supporting Information). Considering that Ca exists only on the surface of silicon as identified by TOF-SIMS, the purity of silicon is estimated at least to be 99.9 wt. % and is expected to be even higher since most of the impurity elements are mainly on the surface.

The elemental mapping of TOF-SIMS is a reasonable indicator of the probable p-type dopant, the distribution of which should show a good match with the silicon domain. Among all elements investigated, only titanium, which is the highest trace impurity in the SiO_2 NPs we used (see Table S2 in Supporting Information), showed a good match with silicon while common p-type dopants, such as B and Al (shallow acceptors) were not detected (Figure 5c). The count ratio of titanium to silicon was around 1:2500. Generally, transition-metal impurities in substitutional silicon sites generate deep acceptor levels in the silicon band gap because of the lack of electrons in the outer sp electron configurations for the formation of four covalent bonds,[11] and therefore, titanium can be a probable p-type dopant in silicon. However, there is a complexity because of the d orbitals of transition metals that can generate many energy levels in the silicon band gap. Titanium in interstitial sites is known to form three deep energy levels; a donor, an acceptor, and a double donor.[11–14] As research about titanium doping in silicon is based on doping by diffusion in the silicon wafer or by addition in the Czochralski silicon melt, the same explanation might not be applied to this case where silicon grows in a different way. Interestingly, other impurities in SiO_2 were not detected in addition to titanium (Figure S5 in the Supporting Information) perhaps for two reasons. First, titanium has an exceptionally low diffusivity in silicon (about 10^{-10} $cm^2 s^{-1}$ at 800 °C),[12] and consequently, it would stay inside silicon during the deposition and cooling processes whereas other impurities could diffuse out and form precipitates at the surface, as suggested by the depth profile analysis. Secondly, titanium is another well-known element that can be obtained by the reduction of its oxide in a $CaCl_2$ molten salt,[15] and therefore, titanium could simultaneously be produced and incorporated during reduction whereas other elements might not.

Silicon growth with the formation of silver islands has also been found in chemical vapor deposition (CVD) and is known as the vapor-liquid-solid (VLS) mechanism.[16] In the CVD process, silver or gold substrates catalyze the reduction of silicon tetrachloride, and form silver–silicon or gold–silicon liquid droplets. Further reduction causes the droplet to be supersaturated with silicon and induces the precipitation of silicon crystals in the form of platelets. The growth of silicon electrodeposited from SiO_2 NPs can be explained in a similar way. The difference is that the reactant is not a gas but solid nano-sized particles. Since the electroreduction of solid SiO_2 would occur only at the three-phase boundary (SiO_2/electrode/$CaCl_2$), the complete conversion of SiO_2 to silicon must be kinetically slow,[7] and perhaps the NPs help the reaction to

be faster and easier.[8] Figure 6 shows the schematic diagram of silicon growth by electrodeposition. At the early stages, SiO_2 particles collide and are adsorbed on the surface of the silver electrode where they are reduced to silicon (Figure 6a).

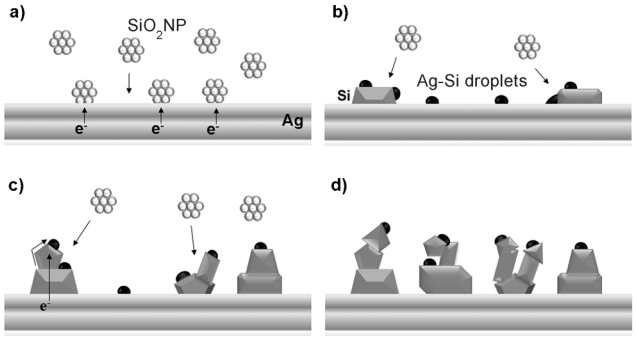

Figure 6. Growth mechanism of electrodeposited silicon.

The reduction creates the silver–silicon liquid drop as well since the operating temperature (850 °C) is slightly above the eutectic temperature of silver–silicon (Ag 89 wt.% and Si 11 wt.%, 835 °C; Figure 6b). As shown in Figure 2a, many silver (or silver–silicon) droplets were found on a silicon surface at the initial stage of electrodeposition. Further reduction leads to the supersaturation of silicon in the droplet and subsequent precipitation and silicon growth (Figure 6c and 6d). The concept of supersaturation and precipitation has been introduced in Ge electrodeposition through a Ge/Hg amalgam which leads to the formation of nanostructured polycrystalline Ge.[17] Contrary to the CVD process, electrodeposition requires continuous supply of electrons passing through the deposit. This could be satisfied with the increase in the conductivity of silicon at high temperature ($\rho >$ 0.05 Ω cm at around 800 °C) and by an increase in the carrier density.[18] In general, electrodeposition proceeds with the nucleation, the formation of the continuous film on the substrate and their growth of the deposit surface for the continuous film growth. In case of silicon electrodeposition from SiO_2, however, the silicon surface did not facilitate the nucleation and the formation of silicon in good quality,[8] and therefore, the generation of silver droplet as a catalytic site is essential for the continuous growth of silicon. Because the growth and crystallization of silicon takes place through silver islands, contrary to general electrodeposition, the morphology of the silicon deposit did not change with the applied potential (Figure S7 in the Supporting Information). This mechanism makes it possible to grow a relatively pure silicon film even though the electrode is surrounded by molten salt and the silicon precursor, which are not pure (99.5%). The reduction on a silver surface prevents the incorporation of $CaCl_2$ directly into silicon, and many impurities would be segregated from the silicon precipitate in the silver–silicon droplet.

Silicon electrodeposition can be used in two ways. One is the use as an alternative process for the production of solar-grade or high-purity silicon which is generally produced through multiple steps which involve carbothermal reduction of SiO_2 (at 2000 °C) followed by the conversion to $SiHCl_3$ or $SiCl_4$ (with HCl at 300 °C) and the hydroreduction to polycrystalline silicon (at 1100 °C). The electrodeposition, however, can produce relatively pure and photoactive silicon directly from the same raw material with a single step, indicating perhaps lower process costs. The other usage would be in the direct fabrication of a thin-film silicon-based solar cell. This would involve the molten salt process being developed in a more convenient way, controlling the doping of the deposit and using silver substrates in the form of thin silver films. Work is in progress to perfect the electrodeposition using higher purity starting materials and conditions.

Received: August 21, 2012
Published online: November 9, 2012

Keywords: electrochemistry · electrodeposition · semiconductors · silicon · solar cells

[1] U. Cohen, *J. Electron. Mater.* **1977**, *6*, 607 – 643.
[2] G. M. Rao, D. Elwell, R. S. Feigelson, *J. Electrochem. Soc.* **1980**, *127*, 1940 – 1944.
[3] R. Boen, J. Bouteillon, *J. Appl. Electrochem.* **1983**, *13*, 277 – 288.
[4] E. J. Frazer, B. J. Welch, *Electrochim. Acta* **1977**, *22*, 1179 – 1182.
[5] T. Munisamy, A. J. Bard, *Electrochim. Acta* **2010**, *55*, 3797 – 3803.
[6] N. Borisenko, S. Z. E. Abedin, F. Endres, *J. Phys. Chem. B* **2006**, *110*, 6250 – 6256.
[7] T. Nohira, K. Yasuda, Y. Ito, *Nat. Mater.* **2003**, *2*, 397 – 401.
[8] S. K. Cho, F.-R. F. Fan, A. J. Bard, *Electrochim. Acta* **2012**, *65*, 57 – 63.
[9] S. R. Herd, P. Chaudhari, M. H. Brodsky, *J. Non-Cryst. Solids* **1972**, *7*, 309 – 327.
[10] H. Ye, H. S. Park, V. Akhavan, B. W. Goodfellow, M. G. Panthani, B. A. Korgel, A. J. Bard, *J. Phys. Chem. C* **2011**, *115*, 234 – 240.
[11] C. A. J. Ammerlaan in *Properties of Crystalline Silicon*, Emis Series No. 20 (Ed.: R. Hull), INSPEC, London, **1999**, pp. 669 – 675.
[12] K. Graff, *Metal Impurities in Silicon-Device Fabrication*, Springer, Berlin, **1995**, p. 112.
[13] A. Rohatgi, J. R. Davis, R. H. Hopkins, P. G. Mcmullin, *Solid-State Electron.* **1983**, *26*, 1039 – 1051.
[14] A. C. Wang, C. T. Sah, *J. Appl. Phys.* **1984**, *56*, 1021 – 1031.
[15] G. Z. Chen, D. J. Fray, T. W. Farthing, *Nature* **2000**, *407*, 361 – 364.
[16] R. S. Wagner, W. C. Ellis, *Appl. Phys. Lett.* **1964**, *4*, 89 – 90.
[17] A. I. Carim, S. M. Collins, J. M. Foley, S. Maldonado, *J. Am. Chem. Soc.* **2011**, *133*, 13292 – 13295.
[18] L. C. Burton, A. H. Madjid, *Phys. Rev.* **1969**, *185*, 1127 – 1132.

